



Computational screening of natural products as tryptophan 2,3-dioxygenase inhibitors: Insights from CNN-based QSAR, molecular docking, ADMET, and molecular dynamics simulations

Yassir Boulaamane ^{a,*} , Santiago Bolivar Avila Jr. ^b , Juan Rosales Hurtado ^c, Iman Touati ^a, Badr-Edine Sadoq ^a, Aamal A. Al-Mutairi ^d, Ali Irfan ^e , Sami A. Al-Hussain ^d, Amal Maurady ^{a,f}, Magdi E.A. Zaki ^d

^a Laboratory of Innovative Technologies, National School of Applied Sciences of Tangier, Abdelmalek Essaadi University, Tetouan, Morocco

^b Institute of Chemistry Rosario (IQUIR, CONICET-UNR) and Faculty of Biochemical and Pharmaceutical Sciences, National University of Rosario, Rosario, Santa Fe, S2002LRK, Argentina

^c National University of Central Buenos Aires Province, Center for Veterinary Research (CIVETAN), Tandil-Argentina, Argentina

^d Department of Chemistry, College of Science, Imam Mohammad Ibn Saud Islamic University (IMSIU), Riyadh, 11623, Saudi Arabia

^e Department of Chemistry, Government College University Faisalabad, Faisalabad, 38000, Pakistan

^f Faculty of Sciences and Techniques of Tangier, Abdelmalek Essaadi University, Tetouan, Morocco

ARTICLE INFO

Keywords:

Parkinson's disease
Tryptophan 2,3-dioxygenase
Natural products
QSAR
Molecular docking
Molecular dynamics

ABSTRACT

Parkinson's disease (PD) is characterised by a complex array of motor, psychiatric, and gastrointestinal symptoms, many of which are linked to disruptions in neuroactive metabolites. Dysregulated activity of tryptophan 2,3-dioxygenase (TDO), a key enzyme in the kynurenine pathway (KP), has been implicated in these disturbances. TDO's regulation of tryptophan metabolism outside the central nervous system (CNS) plays a critical role in maintaining the balance between serotonin and kynurenine-derived metabolites, with its dysfunction contributing to the worsening of PD symptoms. Recent studies suggest that targeting TDO may help alleviate non-motor symptoms of PD, providing an alternative approach to conventional dopamine replacement therapies.

In this study, a data-driven computational pipeline was employed to identify natural products as potential TDO inhibitors. Machine learning and convolutional neural network-based QSAR models were developed to predict TDO inhibitory activity. Molecular docking revealed strong binding affinities for several compounds, with docking scores ranging from -9.6 to -10.71 kcal/mol, surpassing that of tryptophan (-6.86 kcal/mol), and indicating favourable interactions. ADMET profiling assessed pharmacokinetic properties, confirming that the selected compounds could cross the blood-brain barrier (BBB), suggesting potential CNS activity. Molecular dynamics (MD) simulations provided further insight into the binding stability and dynamic behaviour of the top candidates within the TDO active site under physiological conditions. Notably, Penicilherquamide C maintained stronger and more stable interactions than the native substrate tryptophan throughout the simulation. MM/PBSA decomposition analysis highlighted the energetic contributions of van der Waals, electrostatic, and solvation forces, supporting the binding stability of key compounds.

This integrated computational approach highlights the potential of natural products as TDO inhibitors, identifying promising leads that address PD symptoms beyond traditional dopamine-centric therapies. Nonetheless, experimental validation is necessary to confirm these findings.

1. Introduction

Parkinson's disease (PD) is a complex neurodegenerative disorder primarily recognized for its motor symptoms, such as tremor, rigidity,

and bradykinesia [1]. However, non-motor symptoms, including mood disorders, cognitive decline, and gastrointestinal dysfunction, are now understood to significantly impact the quality of life for PD patients and remain poorly managed by traditional dopaminergic treatments [2].

* Corresponding author.

E-mail addresses: boulaamane.yassir@etu.uae.ac.ma (Y. Boulaamane), raailiirfan@gmail.com (A. Irfan), mezaki@imamu.edu.sa (M.E.A. Zaki).

Conventional therapies, such as dopaminergic replacement strategies (e.g., levodopa), aim to restore dopamine levels in the brain to address motor dysfunction [3,4]. While these treatments provide symptomatic relief, they do not halt disease progression or effectively address non-motor symptoms. Moreover, prolonged use of dopaminergic therapies frequently leads to complications such as motor fluctuations and dyskinesia, further limiting their long-term efficacy [5]. These therapeutic limitations highlight the need to explore alternative pathways beyond dopamine replacement.

The kynurenine pathway (KP), the primary route of tryptophan degradation, has emerged as a promising focus due to its role in generating neurotoxic metabolites such as quinolinic acid, which are implicated in neuroinflammation and excitotoxicity in PD [6,7]. Dysregulation of KP enzymes, particularly tryptophan 2,3-dioxygenase (TDO), has been linked to imbalances in neuroactive metabolites [8,9].

In PD, the KP is disrupted due to neuroinflammation, oxidative stress, and mitochondrial dysfunction—hallmark features of disease pathogenesis. This disruption shifts metabolism towards the neurotoxic quinolinic acid instead of the neuroprotective kynurenic acid, contributing to neuronal damage and accelerating disease progression [10].

Activated microglia in PD release inflammatory mediators that upregulate indoleamine 2,3-dioxygenase (IDO) and kynurenine 3-monooxygenase (KMO), directing tryptophan metabolism towards increased quinolinic acid production. Elevated levels of quinolinic acid contribute to neurotoxicity by activating N-methyl-D-aspartate (NMDA) receptors, resulting in calcium influx, excitotoxicity, and neuronal death. In contrast, kynurenic acid acts as an NMDA receptor antagonist, offering neuroprotection against excitotoxic damage [10].

Studies have shown that PD patients exhibit increased quinolinic acid to kynurenic acid ratios, correlating with disease severity and progression. This imbalance highlights KP metabolites as potential biomarkers for early diagnosis and disease monitoring, with elevated quinolinic acid levels reflecting ongoing neuroinflammatory activity [11,12]. While IDO responds primarily to acute inflammation, TDO

contributes to chronic dysregulation of the KP via stress-induced metabolic shifts, exacerbating oxidative stress and serotonin depletion. Targeting TDO may allow long-term metabolic correction by redirecting tryptophan metabolism towards neuroprotective kynurenic acid, reducing quinolinic acid synthesis, and mitigating PD pathogenesis [13].

Given KP's role in PD progression, therapeutic strategies to increase kynurenic acid or inhibit quinolinic acid synthesis may help reduce neurotoxicity and inflammation. These interventions include pharmacological inhibitors of key KP enzymes [13]. Emerging evidence also suggests that the gut microbiota modulates KP metabolism, indicating that probiotics or dietary modifications could complement pharmacological approaches to managing PD symptoms [14].

In Alzheimer's disease, preliminary findings suggest that inhibiting kynurenine production may improve cognitive function in models expressing amyloid precursor protein and tau, further supporting the potential of TDO inhibition to reduce neuroinflammation and metabolic disruption in neurodegenerative diseases [15].

Recent studies have shown that inhibiting TDO can improve disease phenotypes in fruit fly models of AD and PD, leading to enhanced locomotor performance and reduced neurodegeneration. Specifically, pharmacological inhibition using compounds like 680C91, also known as (E)-6-fluoro-3-[2-(3-pyridyl) vinyl]-1H-indole, demonstrated protective effects in these models with a *Ki* value of 51 nM, indicating strong enzyme affinity and competitive inhibition with tryptophan [16].

TDO catalyzes the first and rate-limiting step in the kynurenine pathway by converting tryptophan to N-formylkynurene via an oxidative reaction involving molecular oxygen, as shown in Fig. 1A. This reaction requires a heme cofactor, which binds to TDO's active site and facilitates tryptophan oxygenation. N-formylkynurene then undergoes spontaneous hydrolysis to yield kynurene, a precursor to various downstream metabolites with neurotoxic or neuroprotective effects. The balance between these metabolites, such as the neurotoxic quinolinic acid and the neuroprotective kynurenic acid, is crucial for maintaining neuronal health [17]. Studies have linked elevated kynurene levels

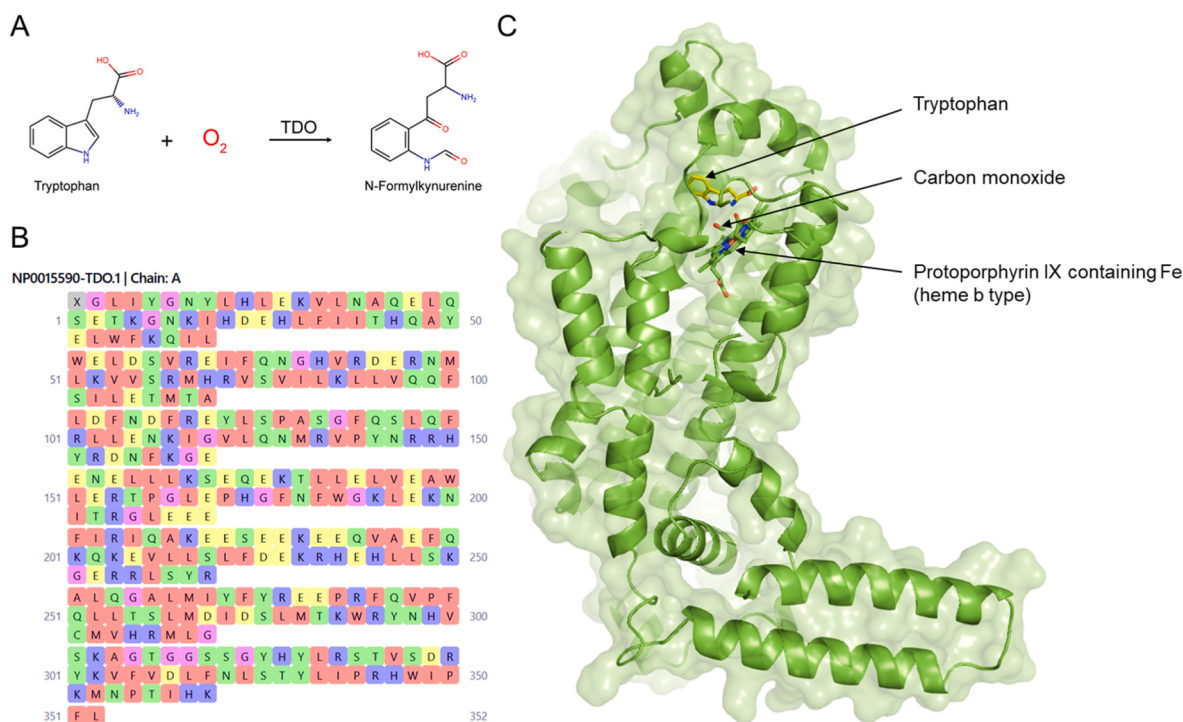


Fig. 1. Visualization of TDO structure and function. (A) The enzymatic reaction catalyzed by TDO, where Tryptophan and molecular oxygen (O₂) are converted into N-formylkynurene. (B) Amino acid sequence of TDO (NP0015590-TDO.1, Chain A) displayed in a color-coded format based on residue properties, highlighting hydrophobic, polar, basic, and acidic residues. (C) 3D structural model of TDO, with key active site components labelled: Tryptophan, Carbon monoxide, and heme b type. (For interpretation of the references to colour in this figure legend, the reader is referred to the Web version of this article.)

and reduced kynurenic acid to PD progression, worsening both motor and non-motor symptoms [18,19]. Consequently, targeting TDO may offer a novel strategy for alleviating PD symptoms, particularly those unresponsive to dopaminergic treatments [20,21].

The amino acid sequence of TDO (Chain A), shown in Fig. 1B, highlights residues color-coded by physicochemical properties—hydrophobic (green), polar (yellow), basic (blue), and acidic (red). Structurally, TDO (PDB ID: 6UD5) features an active site built around a heme b-type cofactor (Fig. 1C) and includes key residues such as HIS-76 and THR-342, which stabilise substrate binding and are essential for catalysis [22]. These residues, along with structural contributors such as GLU-80 and PHE-72, create a specialised environment for enzymatic activity, supporting the rationale for TDO inhibition as a means to reduce neurotoxic metabolite accumulation in PD [23].

Due to the challenges of developing small-molecule drugs that selectively target metabolic pathways without causing significant side effects, natural products are of growing interest for their structural diversity and often favourable pharmacokinetic properties. Natural compounds, including flavonoids and alkaloids, have demonstrated neuroprotective effects, likely through modulation of neuroinflammatory and metabolic pathways such as the KP [24–27]. This study applies an advanced computational framework combining machine learning-based QSAR modelling, molecular docking, ADMET prediction, and molecular dynamics (MD) simulations to screen and

evaluate natural compounds as potential TDO inhibitors. By focusing on TDO inhibition in the context of Parkinson's disease, this pipeline systematically identifies natural products with therapeutic relevance, without requiring CNS-specific activity.

2. Materials and methods

2.1. QSAR modelling

A dataset containing the chemical structures and IC₅₀ values of 1045 compounds experimentally evaluated against TDO (ChEMBL ID: CHEMBL2140) was obtained from the ChEMBL database [28]. Only compounds with activity reported in nanomolar units were selected to ensure data quality. For compounds with multiple activity entries, an average IC₅₀ value was calculated, and a single representative entry was retained using Python's Pandas library (v2.2.0) [29]. After curation, the dataset comprised 859 compounds. The pIC₅₀ values, defined as the negative logarithm (base 10) of IC₅₀ (in molar units), were calculated to transform data into a logarithmic scale, allowing a more linear representation of binding affinities. This transformation compresses the wide range of IC₅₀ values, improving data distribution and facilitating comparison of compound potency.

For classification purposes, compounds with pIC₅₀ values greater than 6 (corresponding to IC₅₀ ≤ 1 μM or 1000 nM) were labelled as

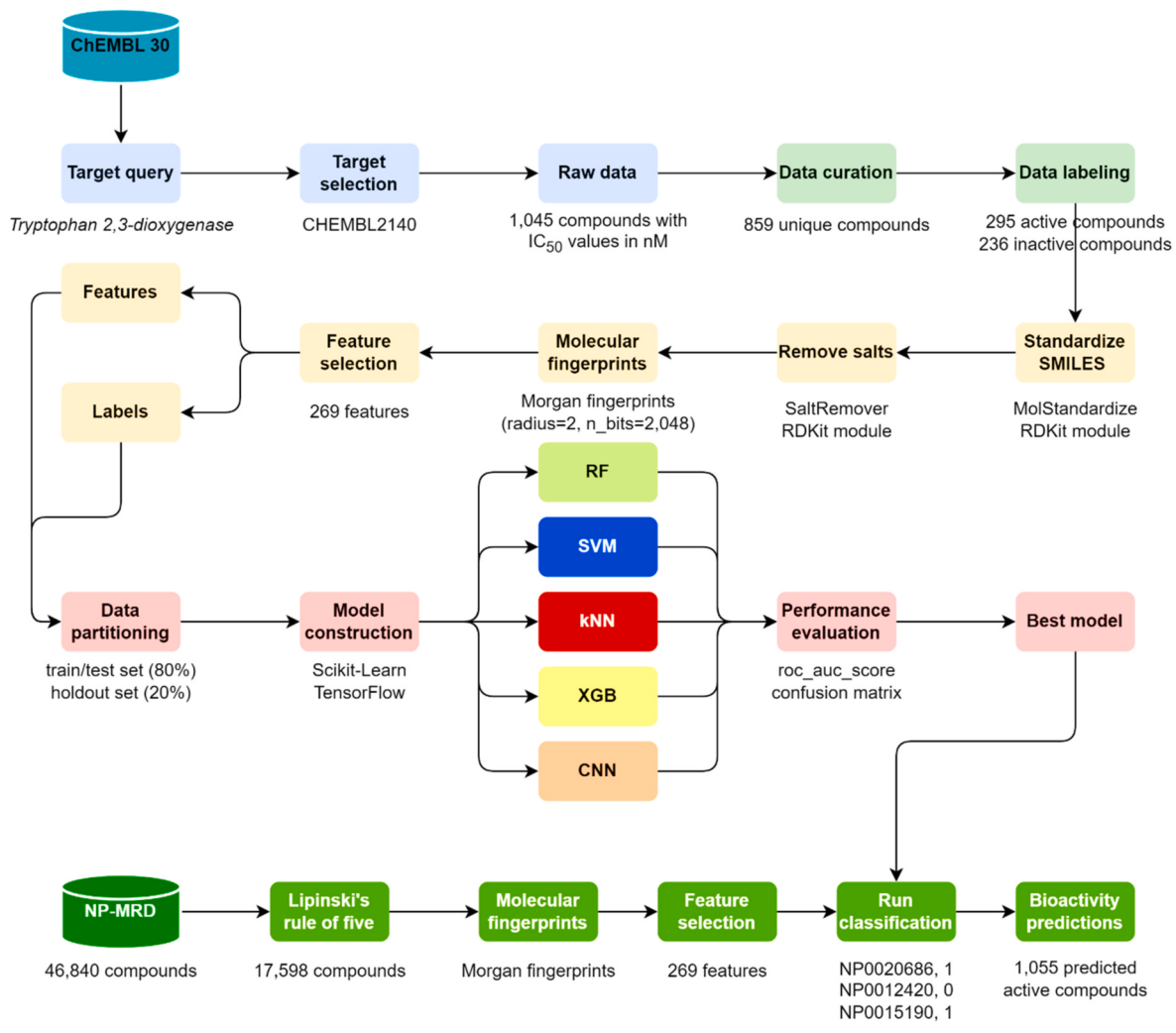


Fig. 2. QSAR workflow for predicting TDO inhibitors. Data preprocessing, feature selection, and model training (RF, SVM, kNN, XGB, CNN) identify bioactive compounds from the NP-MRD database.

active, while those with pIC_{50} values below 5 (corresponding to $\text{IC}_{50} \geq 10 \mu\text{M}$ or $10,000 \text{nM}$) were labelled as inactive, resulting in 295 active and 236 inactive compounds. Compounds with intermediate values were excluded to reduce ambiguity in classification. Morgan fingerprints were generated using the RDKit cheminformatics suite to encode the structural features of each compound (v2023.09.4). [30,31]. These 2048-bit circular fingerprints with a radius of 2 capture atom connectivity and local chemical environments based on the extended-connectivity fingerprint (ECFP4) algorithm. Derived from SMILES representations, they serve as molecular descriptors for model input, effectively representing the molecular structures used in QSAR modelling [31].

The dataset was partitioned into an 80 % combined training/testing set and a 20 % holdout set. The training/testing set was further split into 80 % training and 20 % testing subsets to support QSAR model development and evaluation. The holdout set was reserved exclusively for the final assessment of model performance on unseen data. The complete QSAR workflow (Fig. 2) and associated code are available on GitHub (<https://github.com/yboulaamane/QSARBioPred/>) [32]. The dataset used in this study has also been made publicly available on Zenodo (<https://zenodo.org/records/14591284>).

The QSAR models were evaluated using a comprehensive set of classification metrics, including sensitivity (Eq. (1)), specificity (Eq. (2)), precision (Eq. (3)), negative predictive value (NPV) (Eq. (4)), F1 score (Eq. (5)), accuracy (Eq. (6)), and Matthews correlation coefficient (MCC) (Eq. (7)), to ensure robust performance across multiple dimensions of predictive accuracy. MCC was selected for its effectiveness in handling imbalanced datasets, as it considers all elements of the confusion matrix and provides a balanced evaluation of model performance. The F1 score was included to assess the harmonic mean of precision and recall, helping to minimise both false positives and false negatives. These metrics provided insights into the models' ability to reliably distinguish between active and inactive compounds, supporting their application in virtual screening for potential TDO inhibitors.

$$\text{Sensitivity} = \frac{\text{TP}}{(\text{TP} + \text{FN})} \quad (1)$$

$$\text{Specificity} = \frac{\text{TN}}{(\text{TN} + \text{FP})} \quad (2)$$

$$\text{Precision} = \frac{\text{TP}}{(\text{TP} + \text{FP})} \quad (3)$$

$$\text{NPV} = \frac{\text{TN}}{(\text{TN} + \text{FN})} \quad (4)$$

$$\text{F1 Score} = \frac{2 \times (\text{Precision} \times \text{Sensitivity})}{(\text{Precision} + \text{Sensitivity})} \quad (5)$$

$$\text{Accuracy} = \frac{(\text{TP} + \text{TN})}{(\text{TP} + \text{TN} + \text{FP} + \text{FN})} \quad (6)$$

$$\text{MCC} = \frac{(\text{TP} \times \text{TN} - \text{FP} \times \text{FN})}{\sqrt{((\text{TP} + \text{FP}) \times (\text{TP} + \text{FN}) \times (\text{TN} + \text{FP}) \times (\text{TN} + \text{FN}))}} \quad (7)$$

2.2. Chemical library preparation

The natural product (NP) library used in this study was sourced from the Natural Products Magnetic Resonance Database (NP-MRD) (<https://np-mrd.org/downloads>), comprising 46,840 compounds, which were downloaded in SMILES format [33,34]. The library was processed in DataWarrior to compute physicochemical properties, with filters applied based on Lipinski's Rule of Five to assess drug-likeness [35,36]. Following filtration, 17,598 NPs remained and were subjected to QSAR screening. Predicted active compounds were further optimised, with 3D conformations generated using OpenBabel and

energy minimised using the Merck molecular force field (MMFF94) at physiological pH, ensuring structural stability and suitability for docking and subsequent analyses [37,38].

2.3. Molecular docking

Molecular docking was performed on the 3D crystallographic structure of the TDO enzyme, obtained from the RCSB Protein Data Bank (PDB ID: 6UD5; 2.05 Å resolution) [22,39]. Protein preparation involved the removal of water molecules, retaining only chain A for subsequent calculations. The active site coordinates were identified using the CavityPlus server (<http://www.pkumdl.cn/cavityplus/>), centred on the substrate tryptophan in proximity to the heme cofactor, which was retained during docking due to its essential role in dioxygenase activity with substrates [40]. The grid box was centred at (x, y, z): 39.75, -61.25, -34.0, with dimensions of 16.5 Å × 23.5 Å × 18.0 Å. Molecular docking of the natural compounds retained from the QSAR screening was conducted using AutoDock Vina 1.2.3 [41,42], automated through a custom Python script ("VinaScreen.py") available on GitHub (<https://github.com/yboulaamane/VinaScreen>). Based on binding affinity, the top poses were extracted and compiled into a CSV file for further analysis.

2.4. ADMET prediction

Drug candidates often fail in clinical trials due to poor ADMET properties. To address this, the pkCSM web server was employed (<https://biosig.lab.uq.edu.au/pkcsdm/>) [43] or *in silico* ADMET predictions, key pharmacokinetic parameters were evaluated, including absorption potential, CNS permeability, metabolism by cytochrome P450 enzymes, and toxicity risks. Early computational assessment provides a rapid, cost-effective strategy to identify compounds with favourable ADMET profiles, thereby enhancing success rates across preclinical and clinical development stages.

2.5. Molecular dynamics simulations

Protein–ligand molecular dynamics (MD) simulations were carried out using GROMACS (v2020.6) [44,45], with input files generated via CHARMM-GUI [46], employing the CHARMM36m force field for proteins and ions, and the TIP3P water model [47]. Energy minimisation was performed using the steepest descent algorithm for 5000 steps to stabilise the structure. Simulations proceeded with canonical (NVT) and isobaric–isothermal (NPT) ensemble equilibrations, maintaining a constant temperature of 300.15 K for 100 ps in the NVT phase, followed by an NPT phase at the same temperature and 1 atm pressure for a further 100 ps [48,49]. A production MD run was then extended to 100,000 ps (100 ns).

The workflow began with energy minimisation and equilibration phases, applying positional restraints on the ligand, its heavy atoms, and the protein backbone. During production, the Verlet cutoff scheme was used, with a 1.0 nm cutoff for Coulomb and van der Waals interactions, within a grid box and an *nlist* set to 10. Energies and logs were saved every 10 ps, accumulating 50 million steps to reach the full 100 ns duration.

MD results were analysed using Matplotlib, including root-mean-square deviation (RMSD), root-mean-square fluctuation (RMSF), hydrogen bonding, radius of gyration (Rg), principal component analysis (PCA), and free energy landscape (FEL) analysis. Molecular Mechanics Poisson–Boltzmann Surface Area (MM/PBSA) free energy calculations were conducted following the protocol described by Barraza and colleagues [50]. Final graphs were generated using Matplotlib, which was employed to produce publication-quality plots and to customise each figure for clarity and consistency, enabling detailed insights into the MD simulation results.

3. Results and discussion

3.1. QSAR screening

To build the QSAR models, four machine learning classifiers—Random Forest, Support Vector Machine (SVM), k-nearest neighbors (kNN), and XGBoost—alongside a Convolutional Neural Network (CNN) were employed. Hyperparameter optimisation was performed using either RandomisedSearchCV or GridSearchCV for each classifier, with the Adam optimiser used specifically for the CNN model [51,52]. The CNN model, developed for binary classification of molecular sequence data, begins with an embedding layer that transforms input tokens into 300-dimensional vectors. Feature extraction is performed through two convolutional layers with ReLU activation, each followed by max-pooling layers to reduce dimensionality. The resulting feature maps are flattened and passed through a fully connected dense layer, culminating in a single sigmoid-activated output neuron for classification. The model was compiled using binary cross-entropy as the loss function and evaluated based on classification accuracy.

Model performance was visualised using ROC and precision–recall curves, which displayed AUC values and average precision scores, respectively, highlighting the models' ability to distinguish active from inactive compounds. Classification metrics—including sensitivity, specificity, precision, F1 score, and accuracy—are summarised in Table 1 for comparative analysis. The results demonstrate that the CNN model outperformed traditional machine learning classifiers, as illustrated in Fig. 3. The CNN architecture effectively captured local patterns and spatial relationships within the Morgan fingerprints, enabling the identification of substructural features critical for binding activity. Its ability to extract hierarchical features from input data allowed for improved generalisation, resulting in superior predictive performance compared to conventional algorithms. Consequently, the CNN model was selected to predict the inhibitory potential of natural products from the NP-MRD database, based on fingerprint similarity to known TDO inhibitors from ChEMBL. At this stage, 1055 compounds were predicted to be active.

3.2. Validation of the docking protocol

To validate the accuracy of the docking algorithm used in AutoDock Vina, a redocking approach was employed. In this validation process, tryptophan was selected as the reference molecule. Its structure was retrieved from PubChem (CID: 6305) and prepared using the same protocol to compounds from the NP-MRD library [53].

The prepared tryptophan was then docked into the active site, and the resulting docked conformation was superimposed onto the native co-crystallised substrate. The root-mean-square deviation (RMSD) quantifies the structural difference between two molecular conformations by calculating the average deviation of atomic positions. It is commonly used to assess docking accuracy, with lower RMSD values indicating closer alignment between the docked and native conformations—signifying a successful and reliable docking run, as

illustrated in Fig. 4.

3.3. Docking screening results

The docking study identified the top ten molecules with the strongest binding affinity to TDO, as depicted in Fig. 5. These compounds, exhibiting favourable docking scores, were selected as promising candidates for TDO inhibition. The detailed docking results, presented in Table 2, highlight key binding interactions and molecular contacts for each top ligand. These interactions were thoroughly analysed using the Protein–Ligand Interaction Profiler (PLIP) web server (<https://plip-tool.biotecl.tu-dresden.de/>), providing detailed insights into hydrogen bonding and hydrophobic contacts [54]. In the analysis, tryptophan exhibited a docking score of -6.86 kcal/mol, forming hydrogen bonds with HIS-76, GLY-152, and THR-342. Additionally, it engaged in significant hydrophobic interactions with residues such as PHE-72, LEU-147, and ALA-150, and formed a salt bridge with ARG-144. Among the screened natural product compounds, NP0015590 displayed the highest docking score (-10.71 kcal/mol), engaging in hydrophobic contacts with multiple residues, including PHE-72 and LEU-147. Other top compounds, such as NP0020686 and NP0015190, achieved scores of -10.13 and -10.03 kcal/mol, respectively, and exhibited similar patterns of hydrogen bonding and hydrophobic interactions, with some also participating in π -stacking interactions, particularly with HIS-76. Notably, NP0031886 (-10.00 kcal/mol) formed hydrogen bonds with GLU-56 and GLU-80, along with π -stacking interactions with HIS-76.

Compounds such as NP0003590 and NP0042198 also demonstrated strong hydrophobic profiles, interacting with key residues despite lacking salt bridges or π -stacking. These findings reveal the diverse interaction profiles of the top-ranked ligands, characterised by significant hydrogen bonding, hydrophobic contacts, and occasional π -stacking. The interaction profiles were analysed in the context of TDO inhibition mechanisms. Key residues, such as ARG-117, TYR-113, and THR-254, known to stabilise the substrate via ionic and hydrogen bonding, were targeted by the top ligands [23]. These interactions mimic natural substrate (tryptophan) binding and interfere with catalytic activity by obstructing substrate access to the active site. Hydrophobic and π -stacking interactions further stabilise ligand binding, notably in the case of NP0015190, which exhibited stronger and more stable interactions than tryptophan. The interaction patterns observed in this study align with previously reported substrate-binding mechanisms in TDO, reinforcing the biological relevance of the findings. For instance, HIS-76 and ARG-144 have been consistently identified as critical for substrate recognition and stabilisation in earlier studies [23]. Fig. 6 illustrates the docking poses of the top natural product inhibitors within the TDO active site, visualised using Schrödinger's PyMOL (v2.6.0) [55], highlighting key interactions contributing to their binding stability. Each panel (A–F) displays a different ligand (yellow sticks) positioned within the binding pocket (green surface). Notable interactions include hydrogen bonding with HIS-76, THR-342, GLU-56, and SER-151. These molecular features likely underpin the high

Table 1
Performance of the built classification QSAR models for TDO inhibitors.

Dataset	Model	Sensitivity	Specificity	Precision	NPV	F1 Score	Accuracy	MCC
Test set	RF	0.91	0.96	0.96	0.92	0.93	0.94	0.87
	SVM	0.91	0.92	0.91	0.92	0.91	0.92	0.83
	KNN	0.96	0.92	0.92	0.96	0.94	0.94	0.87
	XGB	0.96	0.96	0.96	0.96	0.96	0.96	0.92
	CNN	0.96	0.94	0.94	0.96	0.95	0.95	0.89
Holdout set	RF	0.88	0.97	0.96	0.89	0.92	0.92	0.85
	SVM	0.92	0.92	0.92	0.92	0.92	0.92	0.83
	KNN	0.95	0.97	0.97	0.95	0.96	0.96	0.92
	XGB	0.92	0.97	0.96	0.92	0.94	0.94	0.88
	CNN	0.92	0.97	0.96	0.92	0.94	0.94	0.88

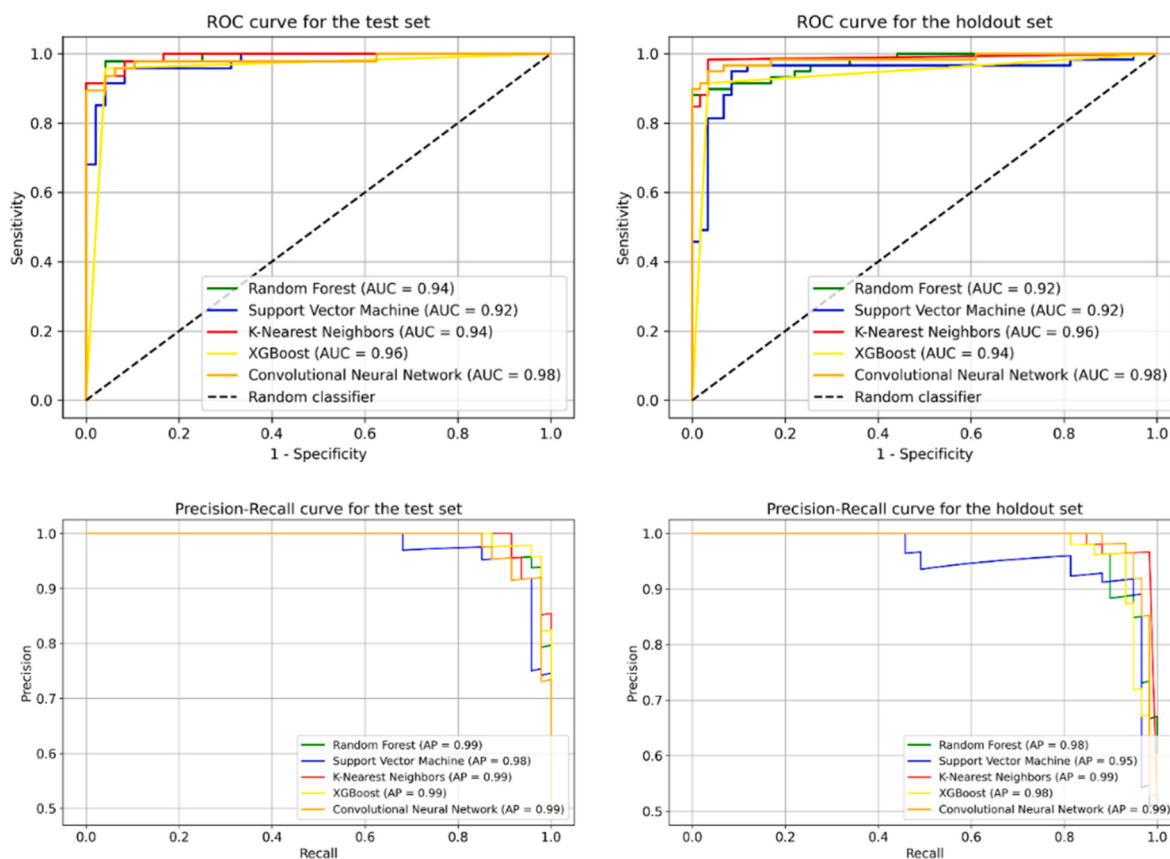


Fig. 3. Performance of machine learning models on classification tasks, shown through ROC (top) and Precision-Recall (bottom) curves for test (left) and holdout (right) sets. The CNN achieves the highest AUC and AP across both sets, indicating superior accuracy and robustness. Models compared include Random Forest, SVM, K-Nearest Neighbors, XGBoost, and CNN.

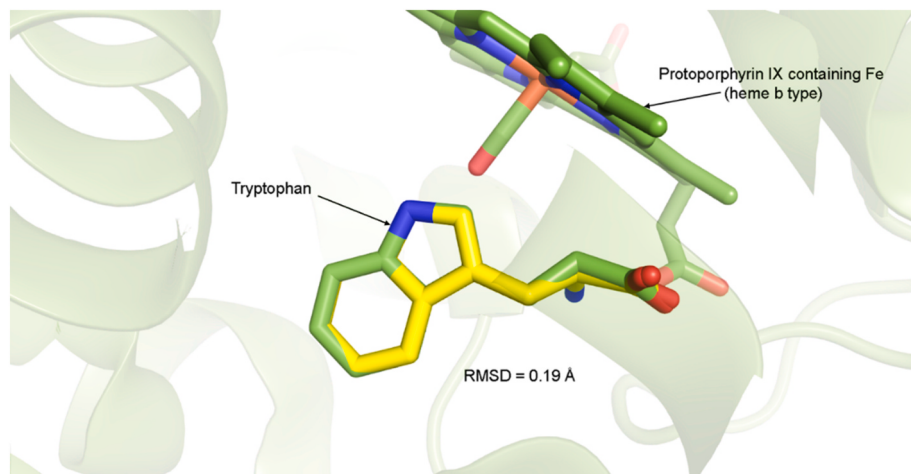


Fig. 4. Redocking results showing the binding interaction between the tryptophan residue and protoporphyrin IX containing Fe (heme b type). The low RMSD of 0.19 Å demonstrates a high level of accuracy in reproducing the binding pose, indicating successful redo.

binding affinities observed, positioning these compounds as promising candidates for further investigation as TDO inhibitors.

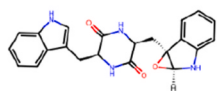
3.4. ADMET results

The ADMET profile analysis, performed using pkCSM, identified several promising candidates for liver-targeted TDO inhibition (Fig. 7). In terms of absorption, all compounds demonstrated poor water solubility, with LogS values below -2 ; notably, NP0031886 showed the

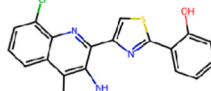
lowest solubility ($\text{LogS} \sim -5$). However, Caco-2 permeability was more favourable, with several compounds, including NP0020686 (~ 1.4), NP0026390, and NP0031764, exhibiting high permeability (> 0.9). Intestinal absorption was generally strong, with most compounds exceeding the 80 % threshold for high absorption, except for NP0031886 and NP0009191.

Regarding distribution, blood-brain barrier (BBB) and CNS permeability data varied across compounds. However, these parameters are less critical in this context, as TDO is predominantly expressed in the

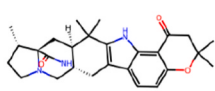
ID: NP0015590
Name: Fellutanine A epoxide



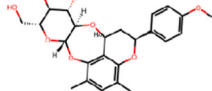
ID: NP0020686
Name: Pyonitrin A



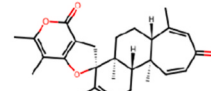
ID: NP0015190
Name: Penicilherquamide C



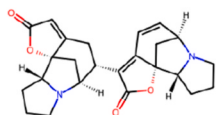
ID: NP0031886
Name: Abacopterin C



ID: NP0003590
Name: Brevione C

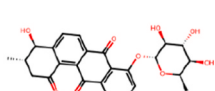


ID: NP0042198
Name: Flueggenine D

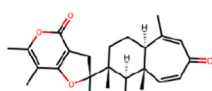


ID: NP0031764
Name: Steronosteroid I

ID: NP0009191
Name: Saccharothrixmicine A



ID: NP0010693
Name: Brevione K



ID: NP0009891
Name: Marinoquinoline E

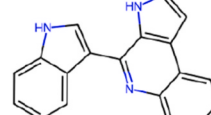


Fig. 5. Top 10 compounds with the highest binding scores from molecular docking against TDO, identified as potential inhibitors.

Table 2

Docking results for top ligands against TDO, detailing their docking scores, key binding interactions, and types of molecular interactions.

Ligand	Chemical class	Docking score (kcal/mol)	H bonds	H bonds distance (Å)	Pi stacking	Hydrophobic interactions	Salt bridges
Tryptophan	Amino acid	-6.86	HIS-76, GLY-152, THR-342	2.30 2.95 2.15	—	PHE-72, LEU-147, ALA-150	ARG-144
NP0015590	Simple indole alkaloid	-10.71	—	—	—	PHE-72, ILE-73, LEU-147	—
NP0020686	Carboline alkaloid	-10.13	SER-151	2.66	HIS-76	GLN-77, GLU-80, PHE-140, LEU-147, THR-342	—
NP0015190	Carboline alkaloid	-10.03	HIS-76	2.91	HIS-76	LEU-147, ALA-150	—
NP0031886	Flavandiol	-10.00	GLU-56, THR-342	2.03 2.65	HIS-76	PHE-72, HIS-76	—
NP0003590	Breviane diterpenoid	-9.96	GLU-80	2.52	—	GLN-58, PHE-72, ILE-73, HIS-76, LEU-147	—
NP0042198	Dimeric securinerga alkaloid	-9.82	—	—	—	PHE-72, ILE-73, HIS-76, LEU-147, ALA-150	—
NP0031764	Steroid glycoside	-9.69	ARG-144, GLY-152, THR-342	2.55 2.93 2.70	—	GLN-58, PHE-72, ILE-73, LEU-147, ALA-150	—
NP0009191	Angucycline	-9.68	GLU-56, GLN-77, GLN-154	3.25 2.61 3.28	—	PHE-72, HIS-76, PHE-140, LEU-147, THR-342	—
NP0010693	Breviane diterpenoid	-9.66	LEU-156	3.00	—	GLU-80, LEU-147, ALA-150	—
NP0009891	Carboline alkaloid	-9.6	SER-151, THR-342	3.71 3.01	HIS-76	PHE-72, HIS-76, PHE-140, LEU-147, THR-342	—

liver. Fraction unbound data revealed that NP0026390 had the highest free drug concentration (~0.6), while other compounds exhibited lower unbound fractions, indicating higher plasma protein binding—potentially beneficial for liver-targeted delivery.

The metabolism analysis identified several key CYP450 interaction patterns that merit further investigation for potential drug–drug interactions. Five compounds (NP0015590, NP0031886, NP0003590, NP010693, and NP0042198) were predicted to inhibit CYP3A4, raising concerns for polypharmacy in PD patients. As CYP3A4 metabolises approximately 50 % of clinically used drugs, including levodopa and dopamine agonists, its inhibition could increase plasma concentrations of co-administered medications, potentially leading to toxicity or adverse effects. These findings highlight the need for detailed *in vitro* enzyme inhibition assays and pharmacokinetic modelling to evaluate the extent of CYP3A4 interaction and inform mitigation strategies, such as dose adjustments or combination therapies.

Additionally, NP0020686 and NP0009891 were predicted to inhibit CYP1A2, while none of the compounds inhibited CYP2D6, which may make them more suitable for CNS-directed applications. These predictions highlight the importance of validating metabolic interactions

through *in vitro* assays and pharmacokinetic models to refine dosing strategies.

Excretion properties varied notably among the compounds. NP0015190 demonstrated high clearance (>0.5 log mL/min/kg), whereas NP0031886 and NP0031764 showed lower clearance rates, indicating differing elimination kinetics that could impact dosing frequency and efficacy.

Toxicity predictions revealed key safety considerations. NP0009891 was flagged for both AMES toxicity and hepatotoxicity. Three compounds (NP0020686, NP0015190, and NP0042198) were predicted to pose hepatotoxicity risks while remaining AMES-negative. The remaining compounds displayed favourable toxicity profiles with no significant alerts for either endpoint.

3.5. Molecular dynamics simulations analysis

The five best ligand–TDO complexes, ranked by binding affinity, along with the reference substrate, were selected for 100 ns MD simulations to evaluate their stability and interaction profiles. The resulting trajectories were analysed using key metrics: root-mean-square

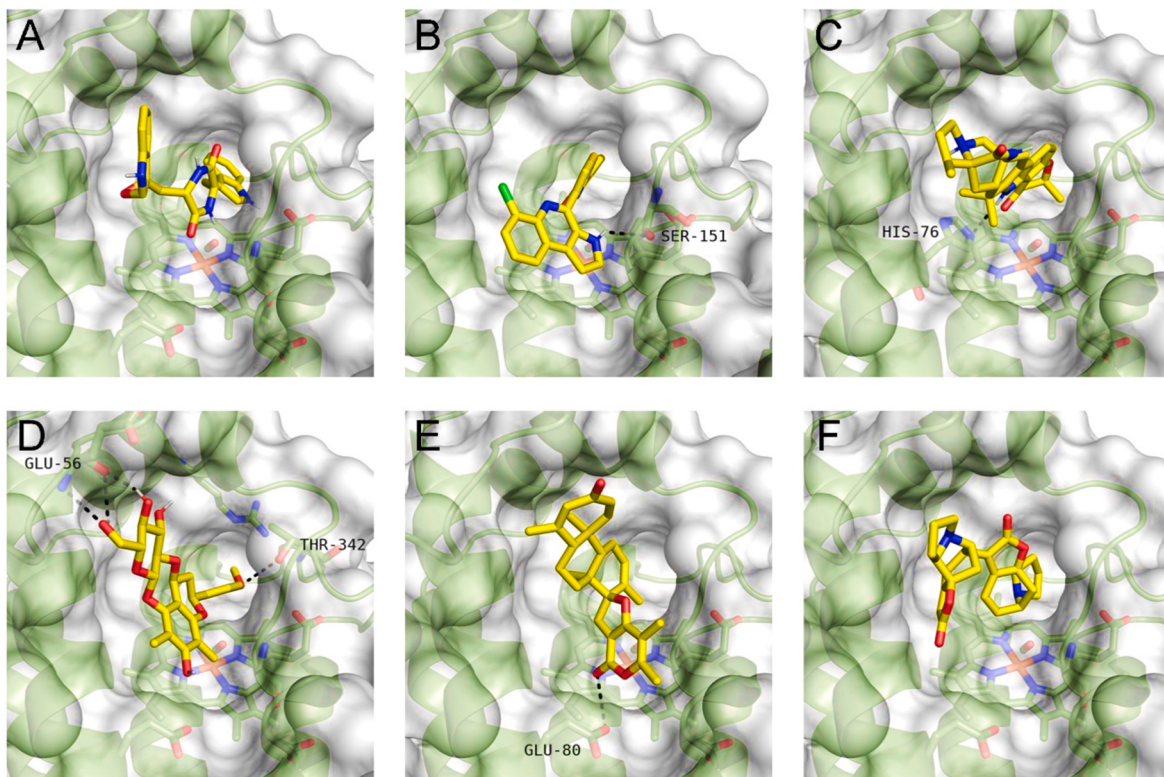


Fig. 6. Docking poses of natural products in the TDO active site. Each panel (A–F) displays a different ligand (yellow sticks) within the binding pocket (green surface). (A) NP0015590, (B) NP0020686, (C) NP0015190, (D) NP0031886, (E) NP0003590, and (F) NP0042198. (For interpretation of the references to colour in this figure legend, the reader is referred to the Web version of this article.)

deviation (RMSD) and root-mean-square fluctuation (RMSF) to assess atomic stability and flexibility; radius of gyration (R_g) to evaluate compactness; solvent-accessible surface area (SASA) to examine hydration effects; and hydrogen bond analysis to monitor ligand–enzyme interactions throughout the simulation. These metrics provide insights into the dynamic behaviour of each complex, supporting the potential of these natural products as stable TDO inhibitors [56].

3.5.1. Root-mean square deviation

RMSD is a valuable metric for analysing the stability of ligand–protein complexes, as it quantifies structural changes in the protein over time during ligand binding. Higher RMSD values indicate greater instability of the complex [57,58]. The RMSD analysis revealed that all complexes exhibited fluctuations of approximately 0.5–2.5 nm (Fig. 8A), except for NP3590, which showed significant deviations reaching up to 9 nm, making it the most unstable ligand in series. A detailed examination of the RMSD plots for each system was conducted to identify the most stable complex. The NP0015190–TDO complex was identified as the most stable. In the early stages of the simulation, this complex displayed fluctuations similar to those of the reference ligand, with values ranging from 0.5 to 2.6 nm. However, beginning at 25 ns, the reference complex showed increased fluctuations between 0.7 and 3.0 nm until approximately 50 ns. In contrast, the NP0015190 complex maintained a more consistent fluctuation range of around 0.6–3.0 nm (Fig. 8B).

3.5.2. Root-mean square fluctuation

Root mean square fluctuation (RMSF) analysis revealed that all ligands studied induced flexibility in similar regions of the protein. Notably, fluctuations between 0.2 and 0.5 nm were observed in the region spanning atoms approximately 1500–2000. Additional flexibility was recorded between atoms 3000 and 3500, reaching up to 0.5 nm, and around atom 5000, where fluctuations ranged from 0.25 to 1.0 nm (Fig. 9A). The NP0015190 ligand exhibited a flexibility profile

comparable to that of the crystallised ligand, with fluctuations ranging from 0.25 to just under 0.5 nm throughout the simulation. Similarly, the crystallised ligand showed consistent flexibility behaviour, with values ranging from 0.25 to approximately 0.5–0.6 nm across the duration of the simulation (Fig. 9B).

3.5.3. Radius of gyration

To complement the findings from the RMSF analysis, a detailed examination of the radius of gyration (R_g) was performed. The selected ligand–TDO complexes exhibited varying R_g values throughout the simulation, as illustrated in Fig. 10A. Notably, the NP0015190 complex maintained a smaller radius of gyration compared to the crystallised ligand, with values ranging from 2.45 to 2.5 nm for most of the simulation. In contrast, the crystallised ligand showed slightly higher values, ranging from 2.55 to 2.6 nm (Fig. 10B). Toward the end of the simulation, both ligands converged to similar R_g values. However, the NP0015190 complex exhibited greater fluctuation, with R_g variations of up to 0.5 nm, whereas the crystallised ligand showed more consistent behaviour, with variations limited to around 0.1 nm.

3.5.4. Solvent accessible surface area

Analysis of the solvent-accessible surface area (SASA) revealed that all ligands studied displayed SASA values similar to those of the crystallised ligand, with fluctuations ranging from 200 to 220 nm² after 20,000 ps. However, some variations were observed among the ligands, attributed to their structural differences. These variations enabled certain ligands to adopt more open, solvent-exposed conformations, thereby reducing their interactions with the protein (Fig. 11A).

The most stable ligand, NP0015190, exhibited lower SASA values than the crystallised ligand. While the crystallised ligand maintained an average accessible surface area between 200 and 210 nm², suggesting a stable conformation in terms of solvent exposure, NP0015190 presented consistently lower SASA values. This indicates a more compact structure

**Fig. 7.** ADMET profiles of the top 10 natural products predicted as TDO inhibitors.

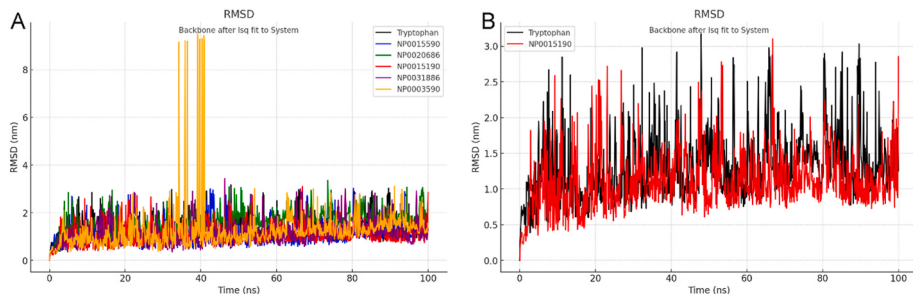


Fig. 8. RMSD analysis of selected molecules in the TDO Protein (a), comparing the NP0015190 molecule with the crystallised ligand over the simulation time-frame (b).

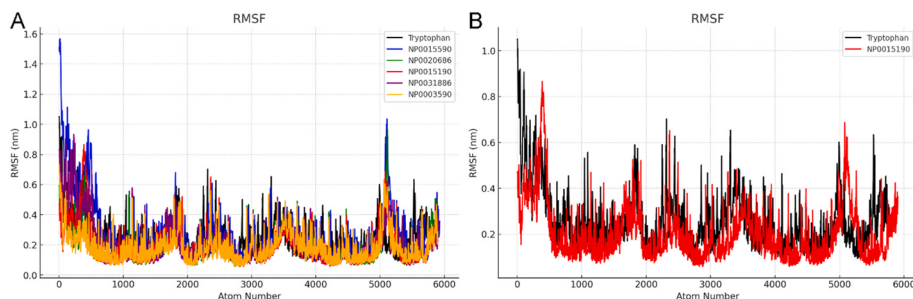


Fig. 9. RMSF analysis shows the flexibility of selected molecules in the TDO Protein (a), with a focus on the NP0015190 molecule and the crystallised Ligand (b).

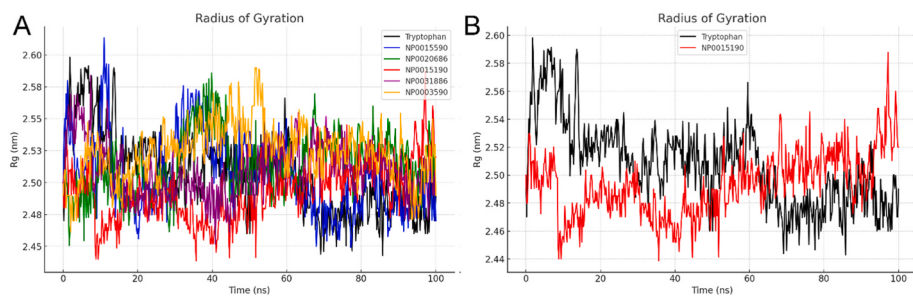


Fig. 10. Comparison of the radius of gyration for the selected molecules in the TDO Protein (a), illustrating the compaction behavior of NP0015190 and the crystallised ligand (b).

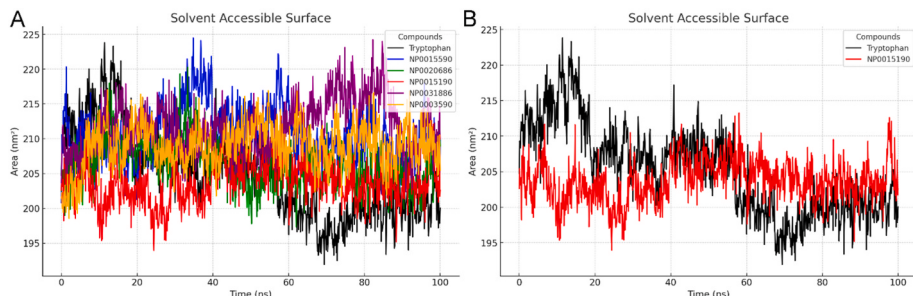


Fig. 11. Comparative SASA profile between the crystallised ligand (reference) (A) and the most stable ligand (NP0015190) (B).

that favours stronger interactions with the protein. The reduced solvent exposure suggests that NP0015190 may possess superior affinity and stability at the protein's active site compared to both the crystallised ligand and the other compounds evaluated (Fig. 11B).

3.5.5. Hydrogen bonds

Finally, analysis of the hydrogen bond profiles from the simulation revealed that the high-affinity compounds formed between 1 and 7

hydrogen bonds throughout the simulation (Fig. 12). Notably, the most stable ligand formed only 1 to 2 hydrogen bonds, a behaviour closely resembling that of the crystallised ligand.

3.5.6. Principal component analysis

The PCA plots in Fig. 13 illustrate the conformational dynamics of the analysed complexes based on PC1 and PC2, highlighting differences in their stability and structural flexibility. The reference tryptophan

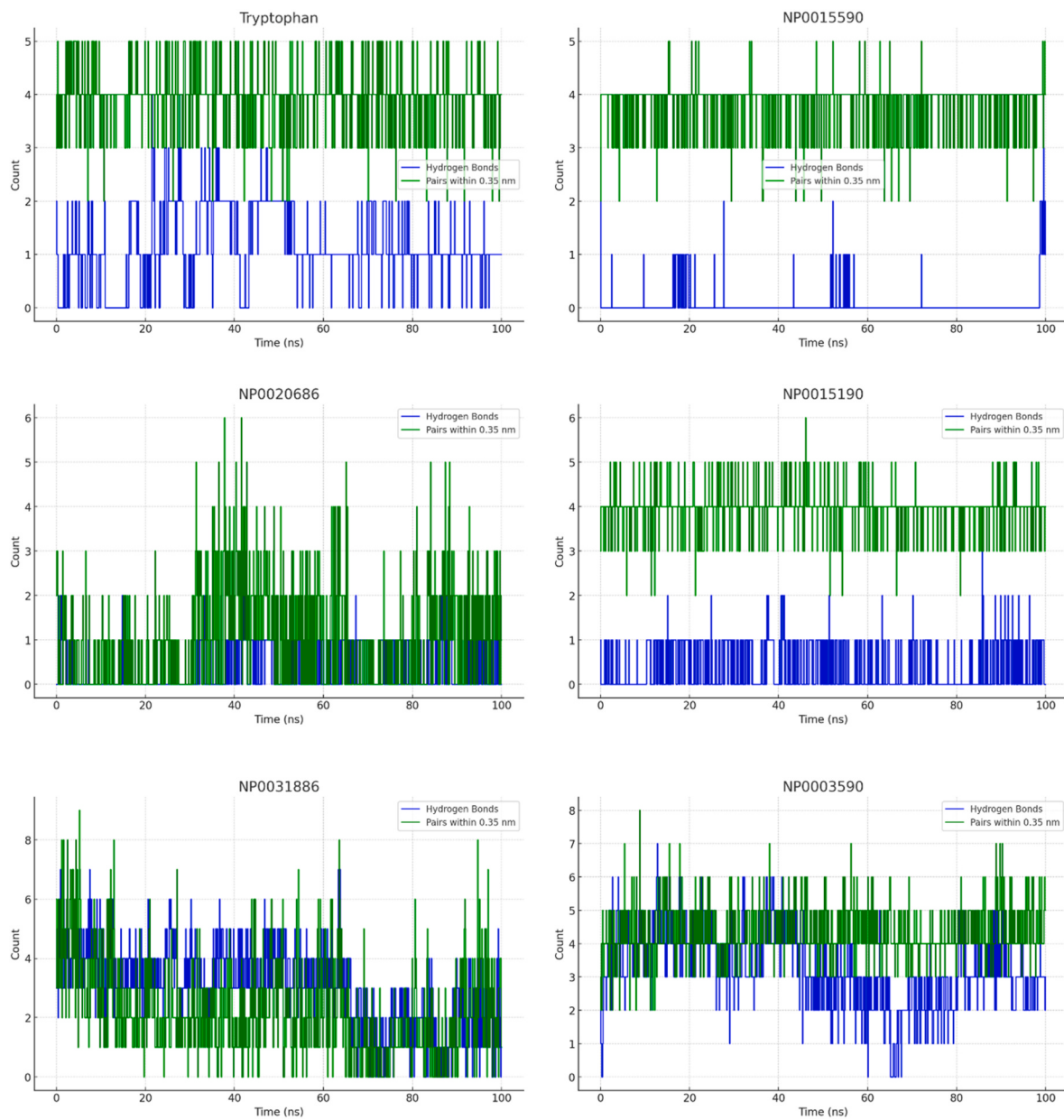


Fig. 12. Hydrogen bond formation diagrams for the selected ligands in complex with TDO Protein during 100 ns simulation time.

complex occupies a relatively compact phase space, indicating stable behaviour and serving as a benchmark for evaluating the other complexes. Among the compounds studied, NP0015590 exhibits the most stable cluster with the smallest phase space occupation, supporting its high binding affinity and reinforcing its potential as a highly stable complex. Similarly, NP0015190 demonstrates notable stability, with its cluster closely resembling that of the tryptophan reference, but with fewer conformational changes—further supporting its structural reliability. In contrast, complexes such as NP0031886 and NP0020686 occupy a broader phase space, suggesting greater conformational variability and reduced stability. These findings reflect the varying degrees of structural stability and flexibility among the tested compounds under the simulated conditions.

3.5.7. Free energy landscape analysis

The 3D free energy landscapes (FELs) for tryptophan and the selected ligands (NP0015590, NP0020686, NP0015190, NP0031886, and NP0003590), shown in Fig. 14, provide detailed insights into their

conformational stability and binding affinities. Tryptophan's FEL displays a broad and shallow energy basin, indicative of multiple stable conformational states and significant flexibility. This reflects its adaptability within the TDO active site but may limit its binding specificity compared to ligands with more localised energy minima.

In contrast, NP0015590 exhibits a deep and well-defined energy minimum, suggesting a rigid binding conformation with limited flexibility—features that enhance its binding specificity and stability. Similarly, NP0020686 shows a localised and deep energy well, reflecting a specific conformational state with moderate flexibility that could improve adaptability while maintaining specificity. NP0015190, characterised by a prominent asymmetric energy well, suggests a stable preferred conformation with some conformational adaptability, optimising its ability to bind the TDO active site while accommodating structural variations.

On the other hand, NP0031886 and NP0003590 exhibit multiple shallow energy wells, indicative of considerable conformational flexibility. While such flexibility may enable these ligands to bind diverse

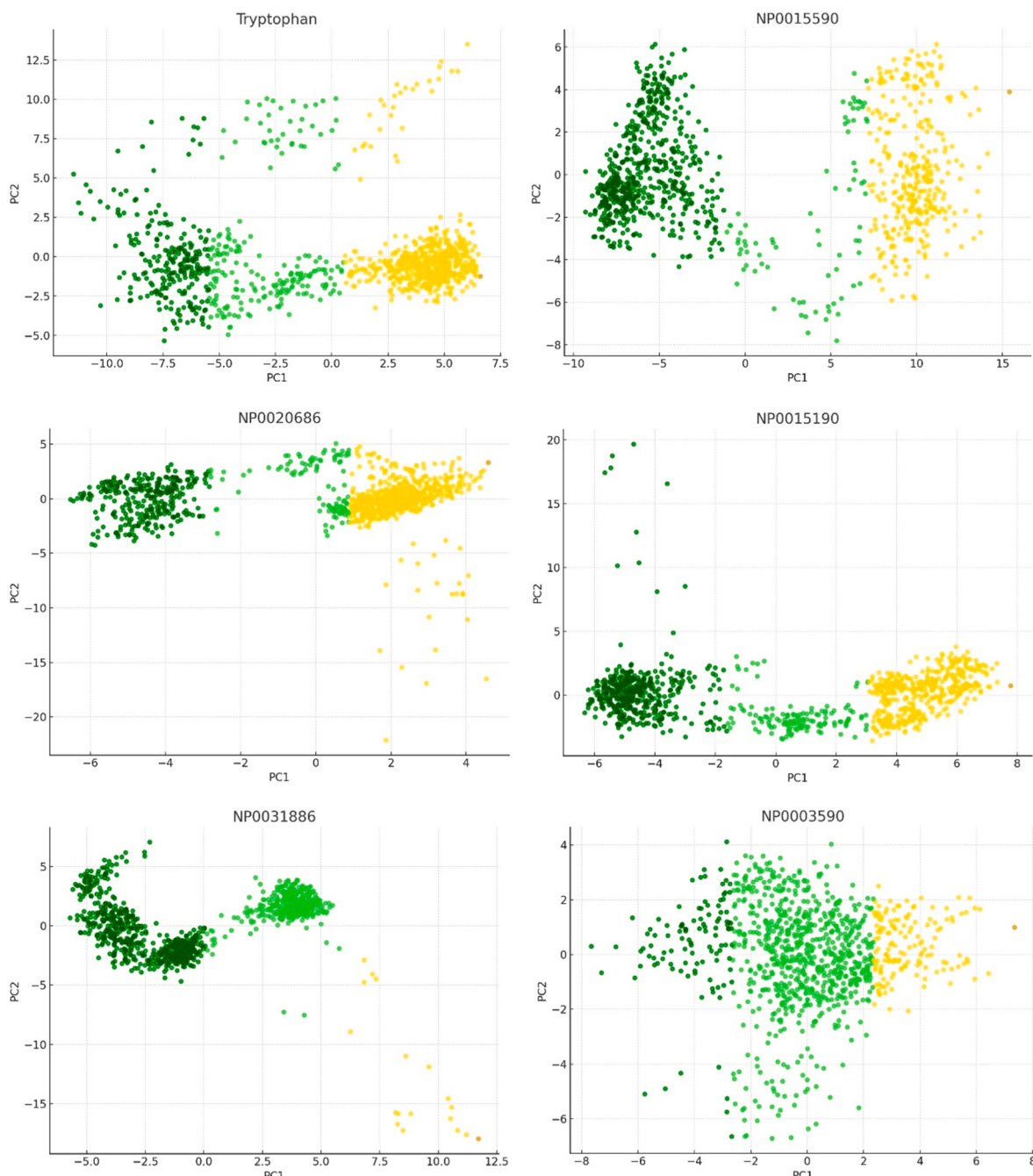


Fig. 13. PCA plots of MD trajectories for Tryptophan and top-ranked ligands. The plots show clustering patterns along PC1 and PC2, highlighting conformational stability and variance of each ligand-TDO complex over the simulation period.

targets or adapt to variations within the binding site, it could compromise binding specificity and stability compared to ligands with deeper minima.

Overall, ligands such as NP0015590 and NP0015190, which possess deep and well-defined energy minima, are more likely to demonstrate strong binding specificity and stability, making them promising candidates for TDO inhibition. In contrast, the greater flexibility observed in NP0031886 and NP0003590 may offer broader target versatility but at the potential cost of specificity. These findings underscore the importance of balancing binding stability and adaptability during lead optimisation in drug design.

3.5.8. MM/PBSA analysis

The MM/PBSA free energy decomposition results, presented in

Table 3, provide insights into the binding affinities and energetic contributions for each studied complex. The binding free energy (ΔG_{bind}) of the natural products indicates stronger interactions with TDO compared to the reference substrate, tryptophan ($-33.40 \pm 18.28 \text{ kcal/mol}$). Among the selected compounds, NP0015190 exhibited the lowest binding energy ($-49.72 \pm 19.96 \text{ kcal/mol}$), suggesting the most stable complex formation.

van der Waals contributions (ΔG_{vdW}) dominated the binding energies across all complexes, underscoring the importance of hydrophobic interactions. For instance, NP0015590 displayed the most favourable ΔG_{vdW} ($-178.78 \pm 14.17 \text{ kcal/mol}$), reflecting strong hydrophobic contacts within the TDO binding pocket. Electrostatic interactions (ΔG_{elec}) varied across the compounds, with NP0003590 showing the strongest contribution ($-41.63 \pm 19.11 \text{ kcal/mol}$),

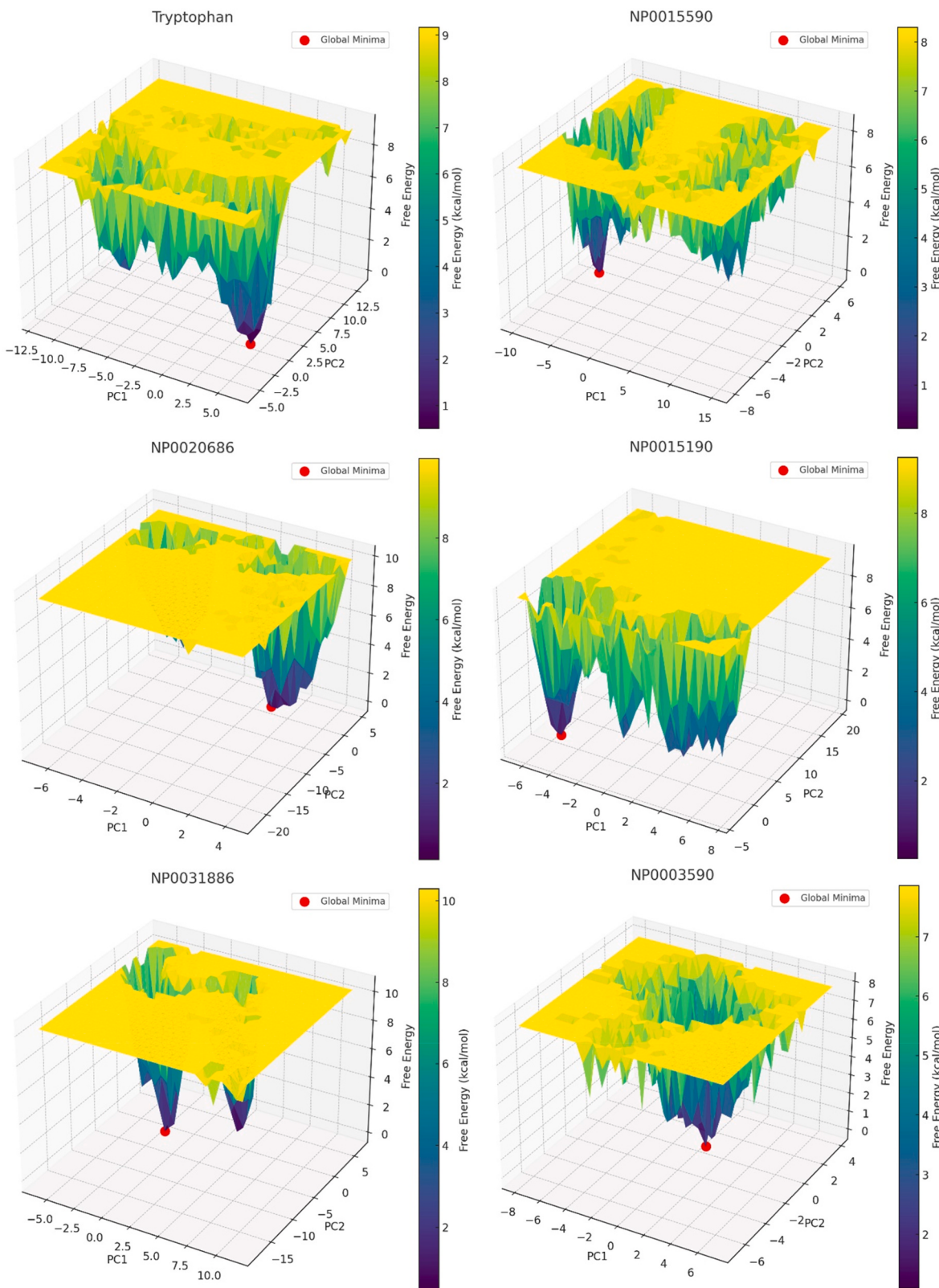


Fig. 14. 3D Free Energy Landscape of Tryptophan and the selected ligands in complex with TDO.

suggesting significant polar and hydrogen-bonding interactions.

In contrast, solvation energy (ΔG_{solv}) partially offset these favourable interactions due to desolvation penalties. This was particularly evident in NP0031886, which showed a high polar solvation energy (158.05 ± 26.58 kcal/mol), potentially affecting overall binding

stability. The solvent-accessible surface area (ΔG_{sasa}) values indicated compact binding, with NP0020686 (-19.87 ± 2.46 kcal/mol) achieving favourable packing within the binding site. Conversely, NP0031886 (-11.04 ± 1.49 kcal/mol) exhibited lower ΔG_{sasa} , reflecting reduced surface exposure and favourable hydrophobic stabilisation.

Table 3

MM/PBSA free energy decomposition results for the studied complexes.

Complex	ΔG_{bind}	ΔG_{vdW}	ΔG_{elec}	ΔG_{solv}	ΔG_{sasa}
Tryptophan	-33.40 ± 18.28	-169.85 ± 12.82	-27.61 ± 13.19	125.22 ± 23.26	-16.48 ± 1.53
NP0015590	-39.90 ± 21.00	-178.78 ± 14.17	-40.31 ± 15.89	136.59 ± 32.34	-13.74 ± 1.77
NP0020686	-44.75 ± 23.62	-172.43 ± 16.42	-28.55 ± 14.13	134.40 ± 32.25	-19.87 ± 2.46
NP0015190	-49.72 ± 19.96	-170.00 ± 15.13	-28.34 ± 15.49	130.77 ± 30.58	-11.04 ± 1.49
NP0031886	-44.63 ± 18.06	-172.53 ± 18.24	-30.23 ± 14.01	158.05 ± 26.58	-14.04 ± 2.82
NP0003590	-47.27 ± 20.68	-170.50 ± 11.53	-41.63 ± 19.11	138.48 ± 31.82	-11.64 ± 2.62

ΔG_{bind} – Binding free energy; ΔG_{vdW} – van der Waals contribution; ΔG_{elec} – Electrostatic contribution; ΔG_{solv} – Solvation energy; ΔG_{sasa} – SASA-based non-polar energy.

The per-residue energy decomposition analysis reveals distinct binding patterns for each compound, as shown in Fig. 15. Tryptophan displays concentrated favourable interactions around residues 54–56 and 64–66, balanced by unfavourable interactions near residues 40–43. NP0015590 exhibits a more complex profile with distributed interactions, showing strong favourable contributions in the 75–80 region and moderate interactions across residues 54–60, alongside some unfavourable interactions in the 85–90 region.

NP0020686 is characterised by two dominant favourable interaction peaks around residues 70 and 135, suggesting a more focused binding mode. NP0031886 shows strong favourable interactions in the 70–75 region, countered by unfavourable interactions across residues 55–65, resulting in a cleaner, more defined interaction profile. NP0015190 presents a notable unfavourable interaction near residue 145, balanced by moderate favourable interactions around residues 80–85, with various smaller contributions across the binding site. NP0003590 features two distinct favourable interaction peaks in the 75–80 region and a significant unfavourable interaction near residue 65, indicating specific key binding points rather than a broadly distributed interaction pattern.

Penicicherquamide C (NP0015190), a secondary metabolite from *Penicillium herquei*, has emerged as a promising natural product for targeting TDO in Parkinson's disease. Structural analysis revealed that its rigidity—attributed to a fused indole and piperazine ring system—enhances lipophilicity and facilitates effective binding within the TDO active site. Key functional groups, including two carbonyl and two amino groups, are likely responsible for stable hydrogen bonding, as supported by MD simulations. From the analyses described above, it can be concluded that the stability of the protein–ligand complex is strongly influenced by the ligand's ability to maintain a compact conformation and minimise solvent exposure (Fig. 11). NP0015190 exhibited this behaviour, evidenced by its low SASA value and reduced flexibility in specific protein regions, thereby contributing to greater complex stability. This was further supported by the formation of up to five hydrogen bonds with active site residues, indicating strong and consistent interactions while preserving the protein's structural integrity (Fig. 12). These findings suggest that NP0015190 can maintain stabilising interactions without compromising structural stability, highlighting its potential as a viable inhibitor of the TDO protein.

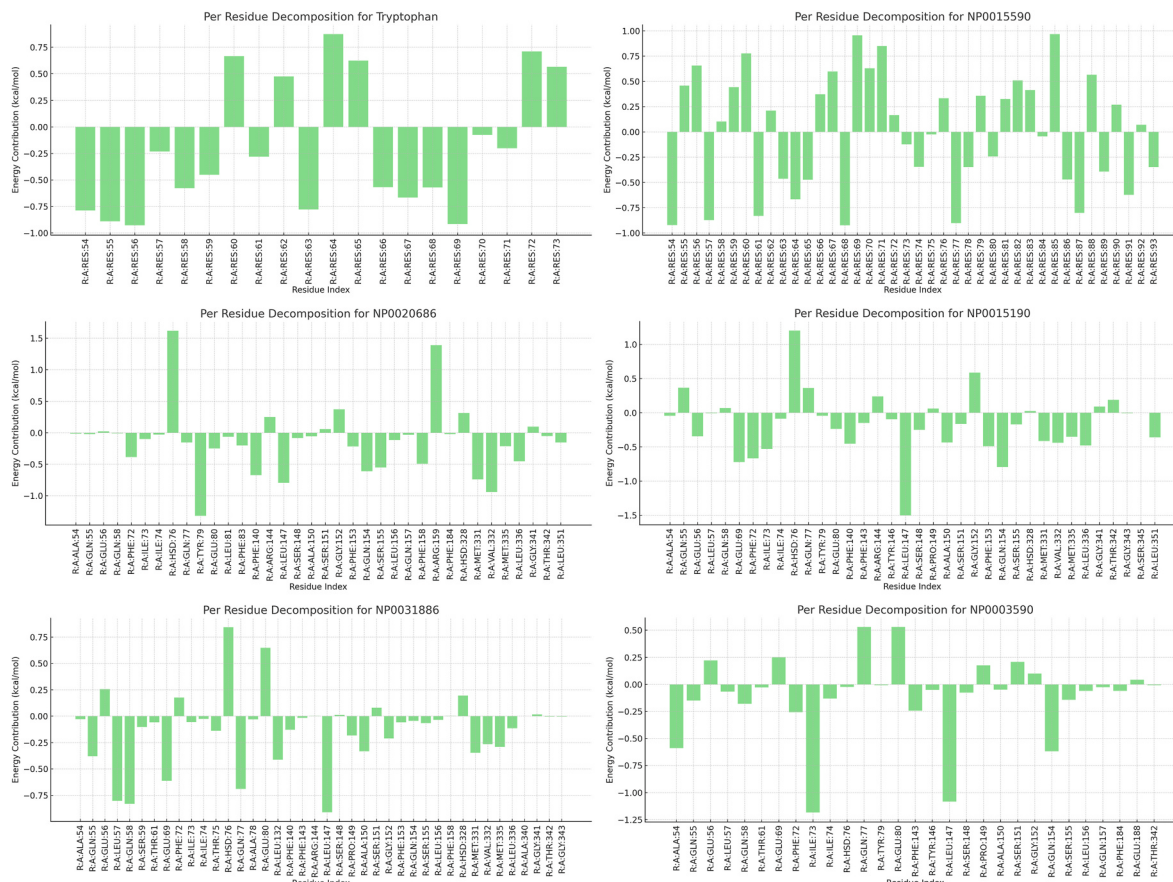


Fig. 15. Per-residue energy decomposition analysis of binding interactions between the compounds studied and their target protein.

While previous studies have explored natural products as TDO inhibitors, our work introduces methodological innovations that significantly advance lead discovery in this field [16,17,59]. Many plant-derived metabolites, including indole alkaloids, glucosinolate derivatives, and quinones, have demonstrated TDO inhibition, often through competitive binding at the active site or interaction with the heme iron. For example, β -carbolines such as harmane and harmine from *Peganum harmala*, and tryptanthrin from *Isatis tinctoria*, exhibit dual indoleamine 2,3-dioxygenase 1 (IDO1)/TDO inhibition, while glucosinolate-derived compounds have been shown to selectively inhibit TDO [60]. Additionally, quinones such as shikonin and dihydrotanshinone I act through allosteric or metal-binding interactions, contributing to their immunomodulatory and anticancer effects [61]. Despite these findings, previous studies have largely focused on compounds already evaluated *in vitro*, limiting the discovery of novel scaffolds with optimised pharmacokinetic properties [62].

To overcome these limitations, we employed a machine-learning-driven QSAR model integrated with molecular docking, ADMET screening, and MD simulations, establishing a multi-level computational pipeline. This approach enables large-scale screening and in-depth validation of natural products, allowing the identification of novel scaffolds such as Peniciherquamide C, which exhibits stronger binding affinities and favourable pharmacokinetic properties compared to known inhibitors. The structural uniqueness of Peniciherquamide C—featuring a fused indole and piperazine ring system—enhances lipophilicity and stabilises interactions within the TDO active site, as confirmed by MD simulations. These findings underscore not only its potential as a TDO inhibitor but also the effectiveness of our computational strategy in broadening the chemical space of natural product-based TDO inhibitors.

In addition to Peniciherquamide C, Fellutanine A epoxide emerged as another promising TDO inhibitor. Structurally, this compound features a unique linked tryptophan-like ring system that resembles two fused tryptophan molecules. Given that TDO naturally binds tryptophan, the structural mimicry of Fellutanine A epoxide suggests a competitive binding mechanism within the active site. Its ability to closely resemble the native substrate reinforces the rationale behind our computational approach and supports its potential as a high-affinity TDO inhibitor. This finding further validates the effectiveness of our pipeline in identifying novel scaffolds that align with known substrate-specific interactions.

Fellutanine A epoxide demonstrated a competitive binding mechanism due to its linked tryptophan-like ring system, which mimics the substrate's natural interactions with TDO. Its docking score and molecular interactions suggest strong binding within the active site, comparable to Peniciherquamide C. However, MD simulations and MM/PBSA analysis revealed distinct stability dynamics, indicating a slightly different mode of stabilisation within the binding pocket. While Peniciherquamide C exhibited greater hydrogen bonding stability, Fellutanine A epoxide showed enhanced van der Waals interactions, which may contribute to a different yet effective inhibition profile. These findings highlight the complementarity of both compounds and further reinforce the effectiveness of our computational pipeline in identifying structurally diverse TDO inhibitors.

Beyond TDO inhibition, Peniciherquamide C has demonstrated notable antiviral activity, with an IC₅₀ of 5.1 μ M against the hepatitis C virus, highlighting its bioactive versatility [63]. These findings further underscore its strong binding affinity, stability within the active site, and favourable ADMET profile, positioning it as a potential lead compound for addressing non-motor symptoms of PD through modulation of the kynurene pathway.

While this study presents a robust computational framework for identifying TDO inhibitors, experimental validation is essential to confirm the predicted inhibitory activity and pharmacokinetic properties. Future *in vitro* assays, such as enzyme inhibition assays, should be conducted to quantify the direct interaction of the identified compounds with TDO. Additionally, cell-based assays could assess their biological

effects in a physiological context, while *in vivo* pharmacokinetic studies would offer insights into their metabolism, bioavailability, and systemic distribution. These steps will be critical for advancing these compounds towards preclinical evaluation.

4. Conclusion

TDO plays a pivotal role in the kynurene pathway, a key metabolic route implicated in Parkinson's disease. Dysregulation of this pathway contributes to an imbalance between neurotoxic and neuroprotective metabolites, exacerbating PD symptoms—particularly those unresponsive to traditional dopaminergic therapies. Targeting TDO offers a promising strategy to restore metabolic balance and alleviate these symptoms.

In this study, Peniciherquamide C (NP0015190), a natural product from *Penicillium herquei*, was identified as a potent TDO inhibitor. Using an integrated computational workflow—encompassing machine learning-based QSAR modelling, molecular docking, ADMET profiling, and MD simulations—the compound demonstrated strong binding affinity, stability within the active site, and favourable pharmacokinetic properties. Its structural features, including a fused indole–piperazine ring system and key functional groups, enhance its interaction profile, as evidenced by molecular simulations.

These findings position Peniciherquamide C as a promising candidate for modulating the kynurene pathway in PD, with the potential to address unmet needs in the management of non-motor symptoms. Beyond its implications for PD, this study highlights the broader utility of natural products in drug discovery and presents a reproducible computational framework for identifying and optimising novel enzyme inhibitors.

Future studies should prioritise experimental validation, structure–activity relationship (SAR) optimisation, and *in vivo* evaluations to assess the safety, efficacy, and CNS permeability of Peniciherquamide C. Moreover, the computational pipeline developed in this study can be adapted to screen inhibitors targeting other metabolic and neurodegenerative pathways. Repurposing existing drugs using this framework may further accelerate the discovery of TDO inhibitors and support the development of innovative therapies targeting oxidative stress, neuroinflammation, and excitotoxicity in diseases such as Alzheimer's and Huntington's disease.

CRediT authorship contribution statement

Yassir Boulaamane: Writing – review & editing, Writing – original draft, Visualization, Validation, Methodology, Investigation, Funding acquisition, Data curation, Conceptualization. **Santiago Bolivar Avila:** Writing – original draft, Visualization, Software, Investigation, Formal analysis. **Juan Rosales Hurtado:** Data curation. **Iman Touati:** Formal analysis. **Badr-Edine Sadoq:** Investigation, Formal analysis. **Aamal A. Al-Mutairi:** Formal analysis. **Ali Irfan:** Supervision, Investigation, Funding acquisition. **Sami A. Al-Hussain:** Project administration, Funding acquisition. **Amal Maurady:** Supervision. **Magdi E.A. Zaki:** Supervision, Resources, Project administration, Formal analysis.

Ethis statement

No human or animal subjects were involved in this study. The research does not include any content that could harm individuals, communities, or the environment. The authors also confirm that the study was conducted with integrity, ensuring transparency, reproducibility, and proper citation of all referenced work.

Declaration of generative AI and AI-assisted technologies in the writing process

During the preparation of this work, the author, Yassir Boulaamane,

used ChatGPT to enhance the clarity and coherence of the manuscript. Following the use of this tool, the author thoroughly reviewed and edited the content as necessary and takes full responsibility for the final content of the publication.

Funding

This work was supported and funded by the Deanship of Scientific Research at Imam Mohammad Ibn Saud Islamic University (IMSIU), Riyadh, 11623, Saudi Arabia (grant number IMSIU-RG23013).

Declaration of competing interest

The authors declare no conflicts of interest relevant to this work. This research was conducted independently, and all opinions, analyses, and conclusions expressed in this publication are those of the authors. No financial, personal, or professional affiliations influenced the design, execution, or interpretation of the study.

Acknowledgments

Authors are thankful to the Deanship of Scientific Research, Imam Mohammad Ibn Saud Islamic University (IMSIU), Saudi Arabia for funding this research.

Part of the results presented in this work have been obtained by using the facilities of the CCT-Rosario Computational Center, member of the High-Performance Computing National System (SNCAD), Mincyt-Argentina.

References

- [1] W. Poewe, et al., Parkinson DISEASE. *Nature reviews disease primers*, Nat. Rev. Dis. Primers 3 (2017) 17014.
- [2] A.H.V. Schapira, K.R. Chaudhuri, P. Jenner, Non-motor features of Parkinson disease, *Nat. Rev. Neurosci.* 18 (7) (Jul. 2017) 435–450, <https://doi.org/10.1038/nrn.2017.62>.
- [3] S. Fahn, The history of dopamine and levodopa in the treatment of Parkinson's disease, *Mov. Disord.* 23 (S3) (Jan. 2008) S497–S508, <https://doi.org/10.1002/MDS.22028>.
- [4] N. Tambasco, et al., Clinical aspects and management of levodopa-induced dyskinesia, *Park. Dis.* 2012, <https://doi.org/10.1155/2012/745947>.
- [5] A. Draoui, O. El Hiba, A. Aimrane, A. El Khiat, H. Gamrani, Parkinson's disease: from bench to bedside, *Rev. Neurol. (Paris)* 176 (7–8) (Sep. 2020) 543–559, <https://doi.org/10.1016/J.NEUROL.2019.11.002>.
- [6] W.Y. Fu, X. Wang, N.Y. Ip, Targeting neuroinflammation as a therapeutic strategy for Alzheimer's disease: mechanisms, drug candidates, and new opportunities, *ACS Chem. Neurosci.* 10 (2) (2019) 872–879, <https://doi.org/10.1021/acscchemneuro.8b00402>.
- [7] R. Gordon, T.M. Woodruff, Neuroinflammation as a therapeutic target in neurodegenerative diseases, *Dis.-Modifying Targets Neurodegener. Disord. Paving Way Dis.-Modifying Ther.* (2017) 49–80, <https://doi.org/10.1016/B978-0-12-805120-7.00003-8>.
- [8] M. Fathi, et al., Dynamic changes in kynurenine pathway metabolites in multiple sclerosis: a systematic review, *Front. Immunol.* 13 (2022), <https://doi.org/10.3389/fimmu.2022.1013784>.
- [9] H. Shen, et al., Therapeutic potential of targeting kynurenine pathway in neurodegenerative diseases, *Eur. J. Med. Chem.* 251 (2023), <https://doi.org/10.1016/j.ejmech.2023.115258>.
- [10] M. Fathi, et al., Dynamic changes in metabolites of the kynurenine pathway in Alzheimer's disease, Parkinson's disease, and Huntington's disease: a systematic Review and meta-analysis, *Front. Immunol.* 13 (Oct) (2022), <https://doi.org/10.3389/fimmu.2022.997240>.
- [11] T. Ogawa, et al., Kynurenine pathway abnormalities in Parkinson's disease, *Neurology* 42 (9) (Sep. 1992) 1702, <https://doi.org/10.1212/WNL.42.9.1702>, 1702.
- [12] D. Venkatesan, M. Iyer, A. Narayanasamy, K. Siva, B. Vellingiri, Kynurenine pathway in Parkinson's disease—an update, *eNeurologicalSci* 21 (Sep. 2020) 100270, <https://doi.org/10.1016/j.ensci.2020.100270>.
- [13] C.K. Lim, et al., Involvement of the kynurenine pathway in the pathogenesis of Parkinson's disease, *Prog. Neurobiol.* 155 (Aug. 2017) 76–95, <https://doi.org/10.1016/j.pneurobio.2015.12.009>.
- [14] P. Chen, X. Geng, Research progress on the kynurenine pathway in the prevention and treatment of Parkinson's disease, *J. Enzym. Inhib. Med. Chem.* 38 (1) (Dec. 2023) 2225800, <https://doi.org/10.1080/14756366.2023.2225800>.
- [15] Z. Ye, L. Yue, J. Shi, M. Shao, T. Wu, Role of Ido and TDO in cancers and related diseases and the therapeutic implications, *J. Cancer* 10 (12) (Jun. 2019) 2771–2782, <https://doi.org/10.7150/jca.31727>.
- [16] M. Salter, R. Hazelwood, C.I. Pogson, R. Iyer, D.J. Madge, The effects of a novel and selective inhibitor of tryptophan 2,3-dioxygenase on tryptophan and serotonin metabolism in the rat, *Biochem. Pharmacol.* 49 (10) (May 1995) 1435–1442, [https://doi.org/10.1016/0006-2952\(95\)00006-1](https://doi.org/10.1016/0006-2952(95)00006-1).
- [17] C. Breda, et al., Tryptophan-2,3-dioxygenase (TDO) inhibition ameliorates neurodegeneration by modulation of kynureine pathway metabolites, *Proc. Natl. Acad. Sci. U. S. A* 113 (19) (2016), <https://doi.org/10.1073/pnas.1604453113>.
- [18] G. Oxenkrug, V. Navrotska, Extension of life span by down-regulation of enzymes catalyzing tryptophan conversion into kynureine: possible implications for mechanisms of aging, *Exp. Biol. Med.* 248 (7) (2023), <https://doi.org/10.1177/1535370223117941>.
- [19] A.T. Van Der Goot, et al., Delaying aging and the aging-associated decline in protein homeostasis by inhibition of tryptophan degradation, *Proc. Natl. Acad. Sci. U. S. A* 109 (37) (2012), <https://doi.org/10.1073/pnas.1203083109>.
- [20] F.A. Boros, L. Vécsai, Tryptophan 2,3-dioxygenase, a novel therapeutic target for Parkinson's disease, *Expert Opin. Ther. Targets* 25 (10) (2021), <https://doi.org/10.1080/14728222.2021.1999928>.
- [21] P. Perez-Pardo, et al., Pharmacological validation of TDO as a target for Parkinson's disease, *FEBS J.* 288 (14) (2021), <https://doi.org/10.1111/febs.15721>.
- [22] K.N. Pham, A. Lewis-Ballester, S.R. Yeh, Conformational plasticity in human heme-based dioxygenases, *J. Am. Chem. Soc.* 143 (4) (2021), <https://doi.org/10.1021/jacs.0c09970>.
- [23] F. Forouhar, et al., Molecular insights into substrate recognition and catalysis by tryptophan 2,3-dioxygenase, *Proc. Natl. Acad. Sci. U. S. A* 104 (2) (2007), <https://doi.org/10.1073/pnas.0610007104>.
- [24] M. Tavan, P. Hanachi, M. de la Luz Cádiz-Gurrea, A. Segura Carretero, M. H. Mirjalili, Natural phenolic compounds with neuroprotective effects, *Neurochem. Res.* 49 (2) (2024), <https://doi.org/10.1007/s11064-023-04046-z>.
- [25] D.W. Lim, J.-E. Lee, C. Lee, Y.T. Kim, Natural products and their neuroprotective effects in degenerative brain diseases: a comprehensive review, *Int. J. Mol. Sci.* 25 (20) (Oct. 2024) 11223, <https://doi.org/10.3390/ijms252011223>.
- [26] N.S. Mohd Sairazi, K.N.S. Sirajudeen, Natural products and their bioactive compounds: neuroprotective potentials against neurodegenerative diseases, *Evid. Based Complement. Alternat. Med.* 2020 (Feb. 2020) 1–30, <https://doi.org/10.1155/2020/6565396>.
- [27] F. Fei, N. Su, X. Li, Z. Fei, Neuroprotection mediated by natural products and their chemical derivatives, *Neural Regen. Res.* 15 (11) (Nov. 2020) 2008, <https://doi.org/10.4103/1673-5374.282240>.
- [28] A. Gaulton, "ChEMBL: a large-scale bioactivity database for drug discovery," *Nucleic Acids Res.*, vol. 40, pp. 1100–1107.
- [29] W. McKinney, "Pandas: a foundational Python library for data analysis and statistics," *Python High Perform. Sci. Comput.*, vol. 14, no. 9, pp. 1–9.
- [30] G. Landrum, RDKit: a software suite for cheminformatics, computational chemistry, and predictive modeling, *Greg Landrum* 8 (2013).
- [31] D. Rogers, M. Hahn, Extended-connectivity fingerprints, *J. Chem. Inf. Model.* 50 (5) (May 2010) 742–754, https://doi.org/10.1021/CI100050T/ASSET/IMAGES/MEDIUM/CI-2010-00050T_0018.GIF.
- [32] Y. Boulaamane, et al., Antibiotic discovery with artificial intelligence for the treatment of *Acinetobacter baumannii* infections, *mSystems* (May 2024) e00325, <https://doi.org/10.1128/msystems.00325-24>, 24.
- [33] D.S. Wishart, et al., NP-MRD: the natural products magnetic resonance database, *Nucleic Acids Res.* 50 (D1) (Jan. 2022) D665–D677, <https://doi.org/10.1093/nar/gkab1052>.
- [34] D.S. Wishart, et al., The natural products magnetic resonance database (NP-mrd) for 2025, *Nucleic Acids Res.* (Nov. 2024) gkae1067, <https://doi.org/10.1093/nar/gkae1067>.
- [35] C.A. Lipinski, Lead- and drug-like compounds: the rule-of-five revolution, *Drug Discov. Today Technol.* 1 (4) (2004), <https://doi.org/10.1016/j.ddtce.2004.11.007>.
- [36] T. Sander, J. Freyss, M. Von Korff, C. Rufener, DataWarrior: an open-source program for chemistry aware data visualization and analysis, *J. Chem. Inf. Model.* 55 (2) (2015), <https://doi.org/10.1021/ci500588j>.
- [37] T.A. Halgren, Merck molecular force field. I. Basis, form, scope, parameterization, and performance of MMFF94, *J. Comput. Chem.* 17 (5–6) (1996) 2, [https://doi.org/10.1002/SIC1096-987X\(199604\)17:5/6<490::AID-JCC1>3.0.CO](https://doi.org/10.1002/SIC1096-987X(199604)17:5/6<490::AID-JCC1>3.0.CO).
- [38] N.M. O'Boyle, M. Banck, C.A. James, C. Morley, T. Vandermeersch, G. R. Hutchison, Open babel: an open chemical toolbox, *J. Cheminf.* 3 (10) (Oct. 2011) 1–14, <https://doi.org/10.1186/1758-2946-3-33/TABLES/2>.
- [39] A. Kouranov, et al., The RCSB PDB information portal for structural genomics, *Nucleic Acids Res.* 34 (suppl_1) (Jan. 2006) D302–D305, <https://doi.org/10.1093/nar/GKJ120>.
- [40] Y. Xu, et al., CavityPlus: a web server for protein cavity detection with pharmacophore modelling, allosteric site identification and covalent ligand binding ability prediction, *Nucleic Acids Res.* 46 (W1) (2018), <https://doi.org/10.1093/nar/gky380>.
- [41] J. Eberhardt, D. Santos-Martins, A.F. Tillack, S. Forli, AutoDock Vina 1.2.0: new docking methods, expanded force field, and Python bindings, *J. Chem. Inf. Model.* 61 (8) (Aug. 2021) 3891–3898, https://doi.org/10.1021/ACS.JCIM.1C00203/SUPPL_FILE/C1C00203_SI_002.ZIP.
- [42] O. Trott, A.J. Olson, AutoDock Vina: improving the speed and accuracy of docking with a new scoring function, efficient optimization, and multithreading, *J. Comput. Chem.* 31 (2) (Jan. 2010) 455–461, <https://doi.org/10.1002/JCC.21334>.
- [43] D.E.V. Pires, T.L. Blundell, D.B. Ascher, pkCSM: predicting small-molecule pharmacokinetic and toxicity properties using graph-based signatures, *J. Med. Chem.* 58 (9) (May 2015) 4066–4072, https://doi.org/10.1021/ACS.JMEDCHEM.5B00104/SUPPL_FILE/JM5B00104_SI_001.PDF.

- [44] M.J. Abraham, et al., GROMACS: high performance molecular simulations through multi-level parallelism from laptops to supercomputers, *SoftwareX* 1 (2015) 19–25.
- [45] D. Van Der Spoel, E. Lindahl, B. Hess, G. Groenhof, A.E. Mark, H.J.C. Berendsen, GROMACS: fast, flexible, and free, *J. Comput. Chem.* 26 (16) (Dec. 2005) 1701–1718, <https://doi.org/10.1002/JCC.20291>.
- [46] S.J. Park, N. Kern, T. Brown, J. Lee, W. Im, CHARMM-GUI PDB manipulator: various PDB structural modifications for biomolecular modeling and simulation, *J. Mol. Biol.* 435 (14) (2023), <https://doi.org/10.1016/j.jmb.2023.167995>.
- [47] J. Huang, A.D. Mackerell, CHARMM36 all-atom additive protein force field: validation based on comparison to NMR data, *J. Comput. Chem.* 34 (25) (Sep. 2013) 2135–2145, <https://doi.org/10.1002/JCC.23354>.
- [48] Y. Boulaamane, K. Jangid, M.R. Britel, A. Maurady, Probing the molecular mechanisms of α -synuclein inhibitors unveils promising natural candidates through machine-learning QSAR, pharmacophore modeling, and molecular dynamics simulations, *Mol. Divers.* (Jul. 2023) 1–17, <https://doi.org/10.1007/S11030-023-10691-X/METRICS>.
- [49] Y. Boulaamane, et al., *In silico* discovery of dual ligands targeting MAO-B and AA2AR from african natural products using pharmacophore modelling, molecular docking, and molecular dynamics simulations, *Chem. Afr.* (Sep. 2024) 1–23, <https://doi.org/10.1007/S42250-024-01074-2/METRICS>.
- [50] G.A. Barraza, A.C. Castro-Guijarro, V. de la Fuente Hoffmann, S.J. Bolívar Ávila, M. I. Flamini, A.M. Sanchez, Drug repositioning for rosacea disease: biological TARGET identification, molecular docking, pharmacophore mapping, and molecular dynamics analysis, *Comput. Biol. Med.* 181 (Oct. 2024) 108988, <https://doi.org/10.1016/J.COMBIOMED.2024.108988>.
- [51] Y. Boulaamane, P. Kandpal, A. Chandra, M.R. Britel, A. Maurady, Chemical library design, QSAR modeling and molecular dynamics simulations of naturally occurring coumarins as dual inhibitors of MAO-B and AChE, *J. Biomol. Struct. Dyn.* (2023), <https://doi.org/10.1080/07391102.2023.2209650>.
- [52] Y. Boulaamane, et al., Computational investigation of phytochemicals from aloysia citriodora as drug targets for Parkinson's disease-associated proteins, *ChemistrySelect* 9 (46) (2024) e202403473, <https://doi.org/10.1002/slct.202403473>.
- [53] S. Kim, et al., PubChem 2019 update: improved access to chemical data, *Nucleic Acids Res.* 47 (D1) (Jan. 2019) D1102–D1109, <https://doi.org/10.1093/NAR/GKY1033>.
- [54] S. Salentin, S. Schreiber, V.J. Haupt, M.F. Adasme, M. Schroeder, PLIP: fully automated protein-ligand interaction profiler, *Nucleic Acids Res.* 43 (W1) (2015), <https://doi.org/10.1093/nar/gkv315>.
- [55] L.W. Delano, PyMol: an open-source molecular graphics tool, *CCP4 Newslett. Protein Crystallogr.* 40 (1) (2002).
- [56] D. Benrezkallah, H. Sediki, A.M. Krallafa, The Structural Flexibility of Cold- and Warm-Adapted Enzymes (Endonucleases I) by Molecular Dynamics Simulation, 2021, <https://doi.org/10.3390/ecsoc-24-08387>.
- [57] P. Bhardwaj, G.P. Biswas, N. Mahata, S. Ghanta, B. Bhunia, Exploration of binding mechanism of tricosan towards cancer markers using molecular docking and molecular dynamics, *Chemosphere* 293 (2022), <https://doi.org/10.1016/j.chemosphere.2022.133550>.
- [58] A.M. da Fonseca, et al., Screening of potential inhibitors targeting the main protease structure of SARS-CoV-2 via molecular docking, and approach with molecular dynamics, RMSD, RMSF, H-bond, SASA and MMGBSA, *Mol. Biotechnol.* 66 (8) (2024), <https://doi.org/10.1007/s12033-023-00831-x>.
- [59] A. Kozlova, R. Frédéric, Current state on tryptophan 2,3-dioxygenase inhibitors: a patent review, *Expert Opin. Ther. Pat.* 29 (1) (Jan. 2019) 11–23, <https://doi.org/10.1080/13543776.2019.1556638>.
- [60] N. Eguchi, Y. Watanabe, K. Kawanishi, Y. Hashimoto, O. Hayashi, Inhibition of indoleamine 2,3-dioxygenase and tryptophan 2,3-dioxygenase by beta-carboline and indole derivatives, *Arch. Biochem. Biophys.* 232 (2) (Aug. 1984) 602–609, [https://doi.org/10.1016/0003-9861\(84\)90579-4](https://doi.org/10.1016/0003-9861(84)90579-4).
- [61] W. Guo, et al., Discovery and characterization of natural products as novel indoleamine 2,3-dioxygenase 1 inhibitors through high-throughput screening, *Acta Pharmacol. Sin.* 41 (3) (Mar. 2020) 423–431, <https://doi.org/10.1038/s41401-019-0246-4>.
- [62] R. Bi, X.-N. Yang, H.-F. Zhou, L.-Y. Peng, J.-X. Liu, Q.-S. Zhao, Eleven undescribed alkaloids from the rhizomes of Sinomenium acutum and their Ido1 and TDO inhibitory activities, *Phytochemistry* 200 (Aug. 2022) 113244, <https://doi.org/10.1016/j.phytochem.2022.113244>.
- [63] S. Nishikori, et al., Anti-hepatitis C virus natural product from a fungus, *Penicillium herquei*, *J. Nat. Prod.* 79 (2) (Feb. 2016) 442–446, <https://doi.org/10.1021/ACS.JNATPROD.5B00555>.